

UC Davis

UC Davis Previously Published Works

Title

18F-FSPG PET/CT Imaging of System xC- Transporter Activity in Patients with Primary and Metastatic Brain Tumors.

Permalink

<https://escholarship.org/uc/item/4mm864jg>

Journal

Radiology, 303(3)

ISSN

0033-8419

Authors

Wardak, Mirwais
Sonni, Ida
Fan, Audrey P
et al.

Publication Date

2022-06-01

DOI

10.1148/radiol.203296

Peer reviewed

^{18}F -FSPG PET/CT Imaging of System x_c^- Transporter Activity in Patients with Primary and Metastatic Brain Tumors

Mirwais Wardak, PhD* • Ida Sonni, MD* • Audrey P. Fan, PhD • Ryogo Minamimoto, MD, PhD • Mehran Jamali, MD • Negin Hatami, MD • Greg Zaharchuk, MD, PhD • Nancy Fischbein, MD • Seema Nagpal, MD • Gordon Li, MD • Norman Koglin, PhD • Mathias Berndt, PhD • Santiago Bullich, PhD • Andrew W. Stephens, MD, PhD • Ludger M. Dinkelborg, PhD • Ty Abel, MD, PhD • H. Charles Manning, PhD • Jarrett Rosenberg, PhD • Frederick T. Chin, PhD • Sanjiv Sam Gambhir, MD, PhD • Erik S. Mittra, MD, PhD

From the Department of Radiology, Molecular Imaging Program at Stanford (MIPS) (M.W., I.S., A.P.F., R.M., M.J., N.H., G.Z., N.F., J.R., F.T.C., S.S.G., E.S.M.), Department of Neurosurgery (N.F., S.N., G.L.), and Department of Neurology and Neurological Sciences (N.F., S.N., G.L.), Stanford University School of Medicine, Stanford, Calif; Department of Molecular and Medical Pharmacology, UCLA Ahmanson Biological Imaging Center, David Geffen School of Medicine at UCLA, Los Angeles, Calif (I.S.); Department of Biomedical Engineering, Department of Neurology, University of California, Davis, Calif (A.P.F.); Stanford Bio-X (M.W., G.Z., G.L., F.T.C., S.S.G.) and Departments of Bioengineering (S.S.G.) and Materials Science & Engineering (S.S.G.), Stanford University, Stanford, Calif; Life Molecular Imaging GmbH, Berlin, Germany (N.K., M.B., S.B., A.W.S., L.M.D.); Department of Pathology, Microbiology and Immunology (T.A.) and Department of Radiology and Radiological Sciences, Institute of Imaging Science, Center for Molecular Probes (H.C.M.), Vanderbilt University Medical Center, Nashville, Tenn; and Department of Cancer Systems Imaging, Division of Diagnostic Imaging, The University of Texas MD Anderson Cancer Center, Houston, Tex (H.C.M.). Received September 4, 2020; revision requested November 9; revision received October 6, 2021; accepted November 18. **Address correspondence to** E.S.M., Department of Diagnostic Radiology, Oregon Health & Science University, 3181 SW Sam Jackson Park Rd, Mail Code L340, Portland, OR 97239 (e-mail: mittra@ohsu.edu).

This work was funded by Life Molecular Imaging and the Ben and Catherine Ivy Foundation.

* M.W. and I.S. contributed equally to this work.

Conflicts of interest are listed at the end of this article.

Radiology 2022; 303:620–631 • <https://doi.org/10.1148/radiol.203296> • Content codes: **NR** **MI**

Background: The PET tracer (4S)-4-(3-[^{18}F]fluoropropyl)-L-glutamate (^{18}F -FSPG) targets the system x_c^- cotransporter, which is over-expressed in various tumors.

Purpose: To assess the role of ^{18}F -FSPG PET/CT in intracranial malignancies.

Materials and Methods: Twenty-six patients (mean age, 54 years \pm 12; 17 men; 48 total lesions) with primary brain tumors ($n = 17$) or brain metastases ($n = 9$) were enrolled in this prospective, single-center study (ClinicalTrials.gov identifier: NCT02370563) between November 2014 and March 2016. A 30-minute dynamic brain ^{18}F -FSPG PET/CT scan and a static whole-body (WB) ^{18}F -FSPG PET/CT scan at 60–75 minutes were acquired. Moreover, all participants underwent MRI, and four participants underwent fluorine 18 (^{18}F) fluorodeoxyglucose (FDG) PET imaging. PET parameters and their relative changes were obtained for all lesions. Kinetic modeling was used to estimate the ^{18}F -FSPG tumor rate constants using the dynamic and dynamic plus WB PET data. Imaging parameters were correlated to lesion outcomes, as determined with follow-up MRI and/or pathologic examination. The Mann-Whitney U test or Student t test was used for group mean comparisons. Receiver operating characteristic curve analysis was used for performance comparison of different decision measures.

Results: ^{18}F -FSPG PET/CT helped identify all 48 brain lesions. The mean tumor-to-background ratio (TBR) on the whole-brain PET images at the WB time point was 26.6 ± 24.9 (range: 2.6–150.3). When ^{18}F -FDG PET was performed, ^{18}F -FSPG permitted visualization of non- ^{18}F -FDG-avid lesions or allowed better lesion differentiation from surrounding tissues. In participants with primary brain tumors, the predictive accuracy of the relative changes in influx rate constant K_i and maximum standardized uptake value to discriminate between poor and good lesion outcomes were 89% and 81%, respectively. There were significant differences in the ^{18}F -FSPG uptake curves of lesions with good versus poor outcomes in the primary brain tumor group ($P < .05$) but not in the brain metastases group.

Conclusion: PET/CT imaging with (4S)-4-(3-[^{18}F]fluoropropyl)-L-glutamate (^{18}F -FSPG) helped detect primary brain tumors and brain metastases with a high tumor-to-background ratio. Relative changes in ^{18}F -FSPG uptake with multi-time-point PET appear to be helpful in predicting lesion outcomes.

Clinical trial registration no. NCT02370563

© RSNA, 2022

Online supplemental material is available for this article.

Brain tumors are a heterogeneous group of neoplasms characterized by different histopathologic features, molecular and genetic features, clinical behavior, and prognosis. The imaging modality of choice for brain tumors is gadolinium-enhanced MRI, which remains the reference standard for initial diagnosis and follow-up (1–3). A major limitation of MRI, however, is its nonspecificity in differentiating treatment-related changes from residual or recurrent disease (4).

The most widely used PET radiopharmaceutical in oncology is the glucose analog fluorine 18 (^{18}F) fluorodeoxyglucose (FDG), but its use in neuro-oncology is limited by a low tumor-to-background ratio (TBR). A variety of PET radiopharmaceuticals have been investigated for brain tumor imaging, including amino acid analogs, nucleosides, and radiopharmaceuticals targeting oxidative metabolism, angiogenesis, blood flow, and hypoxia (5,6).

This copy is for personal use only. To order printed copies, contact reprints@rsna.org

Abbreviations

AUC = area under the ROC curve, FDG = fluorodeoxyglucose, ^{18}F -FSPG = (4S)-4-(3- ^{18}F fluoropropyl)-L-glutamate, IHC = immunohistochemistry, ΔK_i = percentage change between the K_i value estimated using the 30-minute dynamic PET data and the K_i value estimated using the dynamic plus WB PET data, MGMT = O-6-methylguanine DNA methyltransferase, ROC = receiver operating characteristic, SUV = standardized uptake value, SUV_{max} = maximum SUV, $\Delta\text{SUV}_{\text{max}}$ = percentage change in SUV_{max} of the brain lesion between the dynamic PET scan (last frame) and WB PET scan, TAC = time-activity curve, TBR = tumor-to-background ratio, WB = whole body

Summary

PET/CT with (4S)-4-(3- ^{18}F fluoropropyl)-L-glutamate had high sensitivity for detecting primary brain cancers and brain metastases and could help predict primary brain tumor outcomes using information from multi-time-point imaging.

Key Results

- The PET tracer (4S)-4-(3- ^{18}F fluoropropyl)-L-glutamate (^{18}F -FSPG) was taken up by both primary brain tumors and brain metastases with high tumor-to-background ratios (range: 2.6–150.3) and allowed better tumor visualization than fluorine 18 fluorodeoxyglucose PET on a visual assessment.
- With multi-time-point PET imaging, relative changes in ^{18}F -FSPG brain tumor kinetics enabled accurate prediction of lesion outcome, as determined on follow-up MRI and/or pathologic examination (overall accuracy = 89% in primary brain tumor group).
- The temporal pattern of ^{18}F -FSPG uptake in lesions with good and poor outcomes was significantly different in the primary brain tumor group ($P < .05$) but not in the brain metastases group.

The ^{18}F -labeled glutamate analog (4S)-4-(3- ^{18}F fluoropropyl)-L-glutamate (^{18}F -FSPG) is a promising tracer for PET imaging (7). The amino acid glutamate and its transporters play an important role in the brain (8). Glutamate acts as a neurotransmitter, and its transporters are present on both neurons and glial cells, regulating both intra- and extracellular glutamate concentrations. Glucose and glutamate (along with its precursor glutamine) are two major energy sources for tumor cell growth and proliferation (7) (Fig E1 [online]). Due to increased rates of energy use by cancer cells, as well as an increased requirement for cysteine for antioxidant purposes, the cystine-glutamate antiporter system x_c^- is upregulated in these cells (9). As system x_c^- plays a crucial role in redox biochemistry, measuring ^{18}F -FSPG retention using PET can provide a useful index of redox status (10). ^{18}F -FSPG is specifically transported via the x_c^- system, as demonstrated by in vitro and in vivo tumor cell studies (7). Favorable pharmacokinetic properties (11,12) and promising results have been reported from animal and prior human studies (13–22), demonstrating the important role of this transporter in cancer and other diseases with redox and reactive oxygen species imbalances.

The aims of this study were to quantify the dynamics of ^{18}F -FSPG uptake in human primary and metastatic brain tumors and to correlate these PET measurements to lesion outcome, as assessed by follow-up MRI and/or histopathologic examination. We hypothesized that lesions that progressed at

follow-up examination would have a different kinetic behavior from lesions that were stable or had a favorable clinical outcome.

Materials and Methods

Study Design and Participant Inclusion

This open-label, nonrandomized prospective study (ClinicalTrials.gov identifier: NCT02370563; U.S. Food and Drug Administration Investigational New Drug application no. 121728) was approved by the local institutional review board and scientific review committee. It also complied with Health Insurance Portability and Accountability Act guidelines. The study took place between November 2014 and March 2016. The study was presented at the neuro-oncology tumor board by the principal investigators. Eligible participants were referred to the study team members, who confirmed eligibility and obtained written informed consent. Life Molecular Imaging (formerly Piramal Imaging), the study sponsor, provided funding and materials for radiolabeling. The authors who were not employees of or consultants for Life Molecular Imaging had control of inclusion of any data and information that might present a conflict of interest for those authors who were employees of or consultants for Life Molecular Imaging.

Eligibility criteria included the following: histologically confirmed primary brain tumor, recurrent brain tumor, or brain metastasis for which the primary tumor was histologically confirmed; a new brain tumor for which histopathologic confirmation was anticipated following enrollment; a Karnofsky Performance Status score greater than or equal to 60; and no clinically relevant deviations in renal function (serum creatinine > grade 2 of the Common Terminology Criteria for Adverse Events version 4.0). Pregnant or nursing women were excluded from the study. Study participants were divided into three categories: grade 4 primary brain tumors, non-grade 4 primary brain tumors, and brain metastasis. Categorization was based on clinical behavior of the tumors and was not prospectively determined.

Radiopharmaceutical Preparation

Synthesis of the precursor and radiolabeling with ^{18}F were performed as previously described (22). The specific activity of ^{18}F -FSPG was greater than 1000 Ci/mmol (>37 000 GBq/mmol), and the final product was sterile and pyrogen-free.

MRI and Data Analysis

MRI scans were acquired using a 3.0-T (Discovery MR750, GE Healthcare) or 1.5-T (Signa HDxt, GE Healthcare) MRI system. Standardized MRI protocols (23) were followed for each participant.

Two board-certified neuroradiologists (N.F. and G.Z., each with >10 years of experience) independently evaluated all brain MRI studies. A malignancy score, indicating the likelihood of malignancy (as compared with treatment effect) and a growth score, indicating changes in size from previous MRI studies, when available, were given for each lesion. Scores ranged from 1 to 5, with higher scores indicating malignancy or an increase in lesion size (Table E1 [online]). Determination

of growth was performed by comparing the study to the most recent prior study, using a criterion of greater than 25% growth in enhancement in a single linear dimension on the two-dimensional slice with the largest tumor cross-section. A greater than 25% increase or decrease in size was considered significant. Discrepancies were resolved by consensus. MRI evaluation was performed with readers blinded to ¹⁸F-FSPG PET/CT results. The first follow-up MRI scans (mean follow-up ± standard deviation, 6.3 months ± 5.0 after ¹⁸F-FSPG PET/CT), and any available subsequent follow-up MRI scans at the time of the consensus read, were used in the evaluation of lesion outcomes, notably in nonsurgical cases.

PET/CT Imaging and Data Analysis

Within 2 weeks of baseline MRI, all participants underwent ¹⁸F-FSPG PET/CT with a Discovery 600 or 690 PET/CT scanner (GE Healthcare). No clinically relevant interventions were made between the two examinations. A single intravenous injection of ¹⁸F-FSPG (mean activity: 289.5 MBq ± 21.5; range: 254.7–350.7 MBq) was administered to the participant. A 30-minute dynamic brain acquisition was performed immediately after tracer injection (52 frames: 24 frames at 5 seconds per frame, then 28 frames at 1 minute per frame) followed by a whole-body (WB) static acquisition from vertex to mid thigh or toes (based on distribution of metastasis) at 60–75 minutes after injection (3 minutes per bed position). A CT scan (120–140 kV; range, 5–85 mAs) was acquired immediately before the dynamic brain and WB PET scans and used for attenuation correction and anatomic localization. Images were reconstructed using an ordered subset expectation maximization algorithm with two iterations and 32 subsets for the Discovery 600 scanner or two iterations and 24 subsets for the Discovery 690 scanner. When clinically indicated, some study participants also underwent a standard-of-care ¹⁸F-FDG PET/CT scan (participants 3, 5, 10, and 23).

The maximum standardized uptake value (SUV_{max}) of the tumor lesions was calculated on the dynamic brain images (last frame [29–30 minutes]) and WB images by manually drawing a volume of interest on the PET images using the PET edge tool of MIM (version 6.5, MIM Software), with manual adjustment as necessary. The volume of interest was also applied to the dynamic brain PET data to extract individual time-activity curves (TACs) for the kinetic analysis. The coregistered MRI scan was used to aid manual volume-of-interest drawing when needed. TBR was obtained by normalizing the tumor SUV_{max} to the background SUV_{max} on contralateral healthy brain parenchyma.

Data generated or analyzed during the study are available from the corresponding author upon reasonable request.

Compartmental Modeling

Kinetic modeling was performed using Kinetic Imaging System software (version 1.0, University of California, Los Angeles). The input function was derived by drawing volumes of interest on the internal carotid arteries and was corrected for partial volume effect (24). A 50% threshold of the tumor

SUV_{max} was used to define the most active part of the tumor. The blood and tumor TACs were used for kinetic modeling, with the tumor TAC weighted by its frame duration at each time point. A three-tissue sequential compartmental model (25) was applied to estimate the five tumor rate constants. No metabolite corrections for the input function were needed, as a previous study showed there are no radiolabeled metabolites of ¹⁸F-FSPG detectable in plasma or urine up to 4 hours after tracer injection (12). The blood volume fraction was fixed at 5%, and k₆ was fixed to less than 0.01. An overview of the kinetic modeling process is shown in Figure E2 (online).

Table 1: Participant Characteristics and Demographics

Characteristic	Value
No. of participants	26
Mean age (y)*	54 ± 12
No. of men	17
No. of women	9
Diagnosis	
GBM	11
Metastatic NSCLC	5
Metastatic melanoma	2
Metastatic TCC	1
Pilocytic astrocytoma (I)	1
Oligodendroglioma (II)	2
Anaplastic astrocytoma (III)	1
Anaplastic oligodendroglioma (III)	2
Lung NET	1
Diagnostic category	
Grade 4	11
Recurrent	7
Newly diagnosed	4
Non-grade 4	6
Recurrent	5
Newly diagnosed	1
Metastatic	9
Recurrent	8
Newly diagnosed	1
Previous treatments[†]	
None	6
Treatment received	20
Surgery	14
Radiochemotherapy	11
Chemotherapy	3
Stereotactic radiosurgery	5
Whole-brain radiation therapy	2
Antiangiogenic treatment	2
BRAF inhibitors	1

Note.—Data are number of participants unless otherwise noted. Roman numerals refer to the World Health Organization grade as described after diagnosis. GBM = glioblastoma multiforme, NET = neuroendocrine tumor, NSCLC = non-small cell lung carcinoma, TCC = transitional cell carcinoma.

* Age is expressed as the mean ± standard deviation.

[†] Detailed characteristics for each participant can be found in Table E1 (online).

The overall influx rate constant K_1 (in milliliters per minute per gram) was estimated using the dynamic PET data and then the dynamic plus WB PET data. The percentage change between these two values for K_1 was calculated and is referred to as ΔK_1 .

Histopathologic and Immunohistochemistry Evaluation

Tumor specimens for histologic and immunohistochemistry (IHC) evaluation were obtained from either stereotactic needle biopsy or tumor surgical resection. Hematoxylin-eosin staining and IHC of the x_{CT} subunit of the x_c^- system were carried out. x_c^- IHC analysis was categorized using a scoring system from 0 to 3 based on the distribution of the staining (Table E1, Fig E3 [online]). Analysis of *IDH-1* mutational status and *O*-6-methylguanine DNA methyltransferase (MGMT) promoter methylation was also conducted. Tissue samples were ideally obtained within 1 year after ^{18}F -FSPG PET, but when this was not available, the tissue sample collected closest to the ^{18}F -FSPG PET scan date was used for the histopathologic and IHC analyses.

Lesion Outcome Analysis

The clinical outcome of each brain lesion was determined by follow-up MRI and, when available, histopathologic examination. The follow-up MRI and histopathologic data were evaluated in consensus by three board-certified physicians (G.Z., S.N., and G.L., each with >10 years of experience) and classified using a scoring system ranging from 1 to 5 (1–2: good outcome, 3–5: poor outcome; see details in Table E1 [online]). The outcome was defined as the status of the lesion at follow-up MRI when compared with baseline MRI. The outcome metric was based on the physicians' impression of what happened to the lesion on subsequent studies. The physicians were blinded to the ^{18}F -FSPG PET/CT results. The standardized uptake value (SUV), TBR, and kinetic parameters were subsequently correlated with tumor pathology and clinical outcome.

Statistical Analysis

A Student *t* test or Mann-Whitney *U* test for independent samples with Bonferroni correction was applied to the data for statistical comparisons as appropriate. A receiver operating characteristic (ROC) curve analysis was used to compare the performance of different decision measures. Statistical analyses were performed using SPSS software (version 21, IBM). The results

are reported as the means \pm standard deviations (unless otherwise noted) and are regarded as statistically significant if $P < .05$.

Results

Participant Sample

Twenty-six participants (mean age: 54 years \pm 12; 17 men) were enrolled in the study. A total of 48 brain lesions were identified on MRI. Relevant demographic and clinical characteristics are summarized in Table 1; detailed participant characteristics are shown in Table E2 (online).

PET/CT and MRI Analysis

^{18}F -FSPG uptake was present in all 48 tumor lesions (mean SUV_{max} on WB PET, 6.8 \pm 6.2) (Table 2), whereas uptake in contralateral healthy brain parenchyma was negligible (mean SUV_{max} on WB PET, 0.27 \pm 0.10). MRI lesion sizes, as measured on transverse sections, were variable (mean long-axis diameter, 15.46 mm \pm 16.79 [range, 0.5–73 mm]; mean short-axis diameter, 10.27 mm \pm 10.86 [range, 0.3–45 mm]). Although mean ^{18}F -FSPG SUV_{max} and TBR were nominally higher in grade 4 tumors than in non-grade 4 tumors and brain metastases, the difference did not reach the level of statistical significance (Fig E4 [online]).

The mean TBR on the WB scans was 26.6 \pm 24.9 (range: 2.6–150.3). Background tracer activity decreased by greater than 40% from the last frame of the dynamic ^{18}F -FSPG PET scan to the WB time point, leading to a high TBR. In the four participants with ^{18}F -FDG PET scans, lesions visible with ^{18}F -FSPG ($n = 7$) were either not ^{18}F -FDG avid or not easily differentiated from the surrounding edematous and/or necrotic tissues described on MRI scans.

Histopathologic, IHC, and Lesion Outcome Analysis

Results of histologic evaluation were available for 19 participants, with 15 samples obtained within 1 year of ^{18}F -FSPG PET. Results of the IHC analysis are summarized in Table E3 (online). Thirteen lesions were described as malignant and given a poor lesion outcome score by the consensus read (outcome rating scale ≥ 3). Six lesions were given a good lesion outcome score (outcome rating scale < 3), either for the absence of cancer cells or for the extensive presence of necrosis and/or radiation-induced changes in the pathologic sample.

Table 2: Summary of ^{18}F -FSPG PET Brain Lesion Analysis

Group	No. of Participants* (No. of Lesions)	Mean Lesion SUV _{max} * SUV _{max} Range	Mean TBR † TBR Range	Good Lesion Outcome	Poor Lesion Outcome
Grade 4	11 (16)	8.9 \pm 8.3 1.8–32.6	33.9 \pm 35.8 8.5–150.3	5	11
Non-grade 4	6 (11)	4.2 \pm 3.3 1.1–11.5	19.3 \pm 13.2 2.7–39.3	2	9
Brain metastases	9 (21)	6.6 \pm 5.1 0.5–15.0	24.7 \pm 18.3 2.6–68.6	17	4
All tumors	26 (48)	6.8 \pm 6.2 0.5–32.6	26.6 \pm 24.9 2.6–150.3	24	24

Note.—Data are numbers of lesions unless otherwise noted. ^{18}F -FSPG = (4S)-4-(3-[^{18}F]fluoropropyl)-L-glutamate, SUV_{max} = maximum standardized uptake value, TBR = tumor-to-background ratio.

* Numbers in parentheses are number of lesions.

† SUV_{max} of brain lesions was measured on the whole-body PET images. Data are listed as mean \pm standard deviation.

For the remaining 29 lesions, lesion outcome analysis was determined by consensus, with the outcome rating score defined by clinical status and findings on follow-up MRI. Eleven lesions were given a poor lesion outcome score, and 18 were given a good lesion outcome score.

IDH-1 mutational status was available for 15 of 17 participants with primary brain tumors, and only one of these participants (participant 16) tested positive for the *IDH-1* mutation.

MGMT status was available for 10 of 17 participants, with four testing positive for MGMT gene promoter methylation (participants 1, 8, 16, and 24).

Group Analysis

¹⁸F-FSPG PET quantitative measures, MRI scores, and lesion outcome scores, as stratified by their diagnostic group category, are summarized in Tables E4–E6 (online). An overview of the

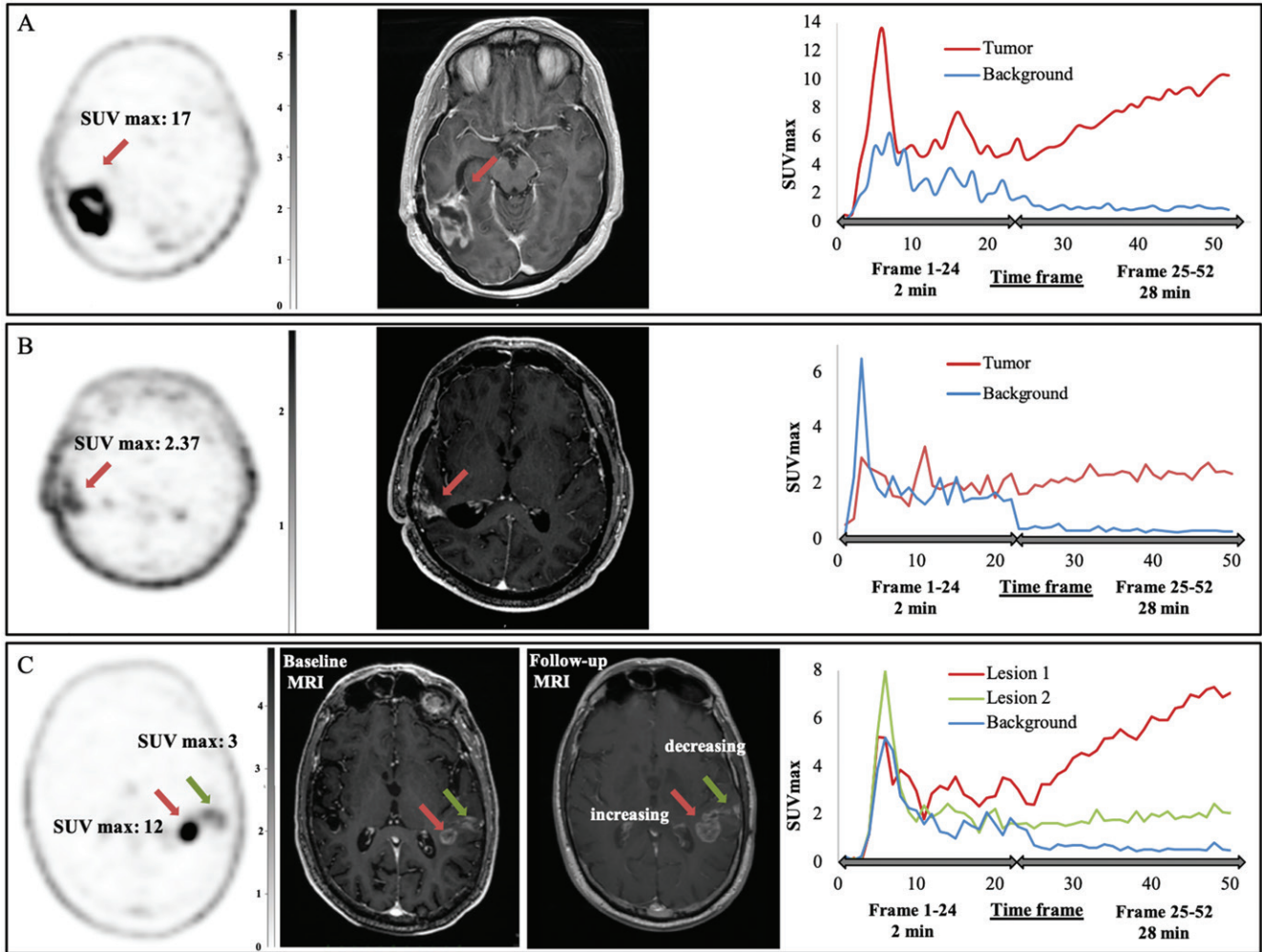


Figure 1: (A) Images in a 63-year-old woman (participant 13) with right temporoparietal glioblastoma multiforme treated with surgery, followed by chemotherapy (temozolomide) and radiation therapy. MRI findings are equivocal for residual disease versus posttreatment change. Static (4S)-4-(3-[¹⁸F]fluoropropyl)-L-glutamate (¹⁸F-FSPG) PET image (left) shows intense uptake in the tumor lesion (arrow), which is visible on the postcontrast three-dimensional spoiled gradient-echo MRI scan (arrow, middle). The tumor time-activity curve (TAC) from the dynamic ¹⁸F-FSPG PET images (right) shows a rapidly increasing uptake over time in the glioblastoma multiforme lesion with an early peak uptake in the first 10 frames. In the background tissue TAC, there is an early peak in the first 10 frames followed by a downward slope and an eventual plateau near zero activity in the final 28 frames. Subsequent pathologic examination confirmed the presence of malignant cells. The outcome score for this lesion was a 5. SUV_{max} = maximum standardized uptake value. (B) Images in a 44-year-old man (participant 4) with glioblastoma multiforme in the right temporal lobe treated with surgery, followed by chemotherapy and repeat resection showing no tumor. MRI scan (middle) shows an area of contrast enhancement concerning for progression (arrow). Static ¹⁸F-FSPG PET image (left) shows weak uptake (arrow). The lesion TAC from the dynamic ¹⁸F-FSPG PET images (right) shows a plateau line after an early uptake peak, and higher uptake values in the tumor lesion at late times when compared to background, with a slight and slow tendency to increase over time. Subsequent pathologic examination showed necrosis and reactive changes with no definite glial neoplasm. The outcome score for this lesion was a 1. (C) Images in a 77-year-old man (participant 2) with grade III unresectable anaplastic astrocytoma of the temporal lobe (post-radiation therapy). Baseline MRI scan (middle) shows a lesion with two separate components, one medial (lesion 1, red arrow) and one lateral (lesion 2, green arrow). Static ¹⁸F-FSPG PET image (left) shows prominent uptake medially (SUV_{max} = 12), and weak uptake laterally (lesion SUV_{max} = 3 on whole body [WB] PET). Follow-up MRI scan (middle) obtained 4 months after baseline shows an increase in size of the medial component, while the lateral component remains stable. In the background volume of interest, the TAC on the dynamic ¹⁸F-FSPG PET scan (right) shows an exponential decaying behavior after an early uptake peak. A similar TAC pattern is seen in the lateral lesion, but with higher uptake values at late times when compared to the background volume of interest, with a slight and slow tendency to increase over time. The medial lesion shows rapidly increasing uptake over time throughout the whole duration of the dynamic PET acquisition. The slight tendency of ¹⁸F-FSPG uptake to increase in the lateral (nonenhancing) component of the tumor, and the mild uptake on the WB late scan (SUV_{max} = 3), suggests a “wait and watch” approach would be best for this lesion. Mild uptake indicates uptake slightly higher than surrounding background (healthy tissue). The outcome score for both lesions in this patient was a 4.

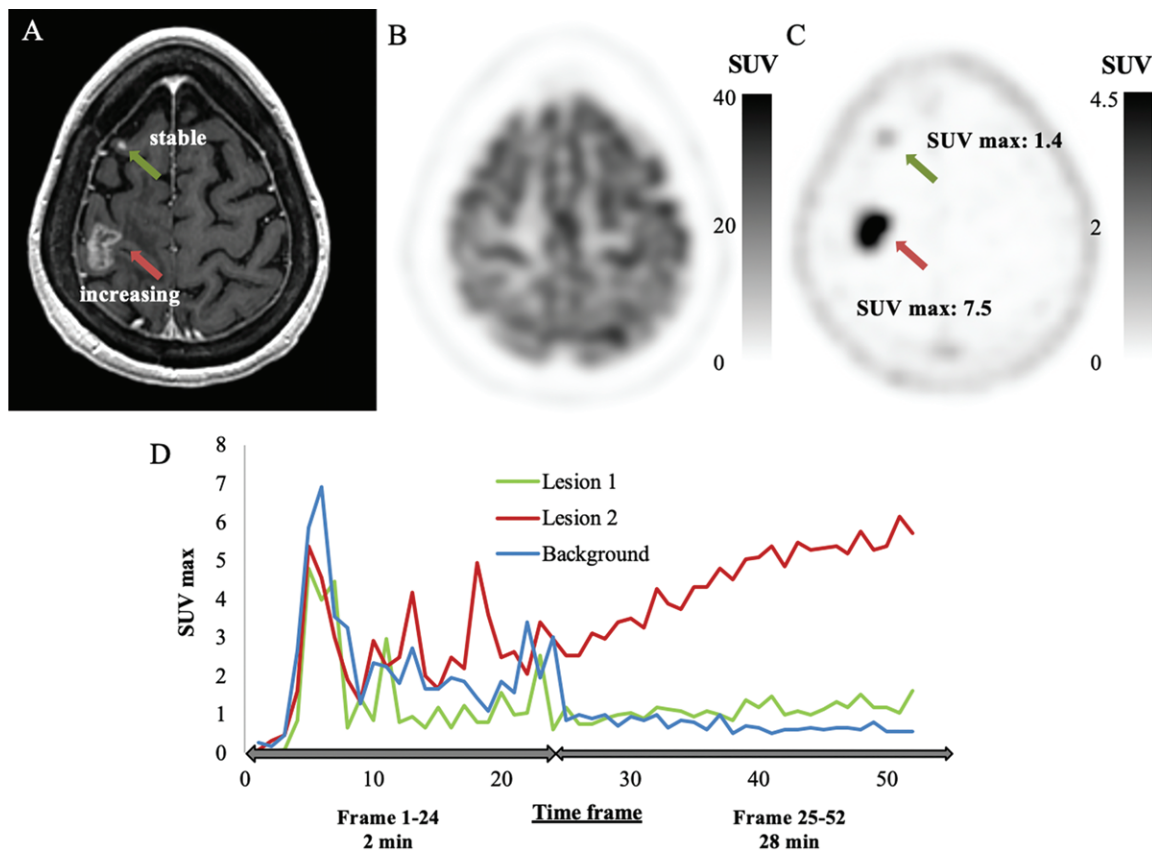


Figure 2: Images in a 65-year-old woman (participant 3) with non-small cell lung cancer brain metastases. **(A)** Contrast-enhanced MRI scan shows a small right frontal lesion (lesion 1, green arrow) and also an enhancing lesion within the right central sulcus (lesion 2, red arrow), which may represent evolving treatment effects or progression. **(B)** Fluorine-18 fluorodeoxyglucose PET image shows no uptake in either lesion, whereas **(C)** (4S)-4-(3-[^{18}F]fluoropropyl)-L-glutamate (^{18}F -FSPG) PET image shows mild uptake in the smaller anterior lesion and intense uptake in the bigger posterior lesion. **(D)** Tissue time-activity curves from the dynamic ^{18}F -FSPG PET images show a plateau line after an early uptake peak in the background volume of interest, and a similar pattern in the small right frontal lesion (lesion 1), whereas the larger lesion in the right central sulcus (lesion 2) shows rapidly increasing uptake over time throughout the whole duration of the dynamic acquisition. The outcome score was 1 for lesion 1 and 2 for lesion 2. SUV = standardized uptake value, SUV_{max} = maximum SUV.

mean results per group is given in Table 2, and examples of ^{18}F -FSPG PET scans, MRI scans, and lesion TACs are shown in Figures 1 and 2. Mean ^{18}F -FSPG lesion TACs of the different brain tumor participant groups are shown in Figures 3 and E5 (online).

Compartmental Modeling

Compartment model-fitted curves are shown in Figure 3. The R^2 values of the fits were greater than 0.94. The influx rate constant K_i was highest in the grade 4 lesions, followed by the brain metastases and the non-grade 4 lesions (Table 3). A similar trend was observed for the k_3 parameter, which describes the transport rate constant of the tracer into the cell by the system x_c^- transporter. In Figure E6 (online), parametric PET images of various biologic kinetic parameters are shown for a 48-year-old man with newly diagnosed glioblastoma (participant 20).

Compartment model-fitted curves for grade 4 primary brain tumor lesions, as stratified by their lesion outcome, are shown in Figure 4. In this group, participants with poor lesion outcomes had a higher positive slope in their tumor curves when compared with participants with good lesion

outcomes. Kinetic analysis showed that the ^{18}F -FSPG rate constant for transfer of tracer into the tumor cells (k_3 ; in min^{-1}) of the poor lesion outcome group was approximately four times greater than that of the good lesion outcome group (mean, 0.875 ± 0.084 vs 0.212 ± 0.091 , respectively). The ^{18}F -FSPG sequestration rate constant k_5 (in min^{-1}) and influx rate constant K_i (in $\text{mL}/\text{min}/\text{g}$) were also larger by twofold in participants with poor versus good lesion outcome scores (mean k_5 , 0.077 ± 0.010 vs 0.035 ± 0.009 , respectively; mean K_i , 0.050 ± 0.012 vs 0.026 ± 0.014).

^{18}F -FSPG uptake analysis results and physician consensus outcome scores for each participant's lesion are summarized in Table E7 (online). SUVs measured at single time points on the dynamic PET (last frame) or WB PET were found to be suboptimal in predicting good or poor lesion outcome on follow-up examination using ROC curve analysis. This was similarly true for the K_i values estimated using the 30-minute dynamic PET data or the dynamic plus WB PET data.

Although both ΔK_i and the relative change in SUV_{max} between the dynamic PET (final frame) and WB PET (referred to as $\Delta\text{SUV}_{\text{max}}$) performed well in separating the two lesion

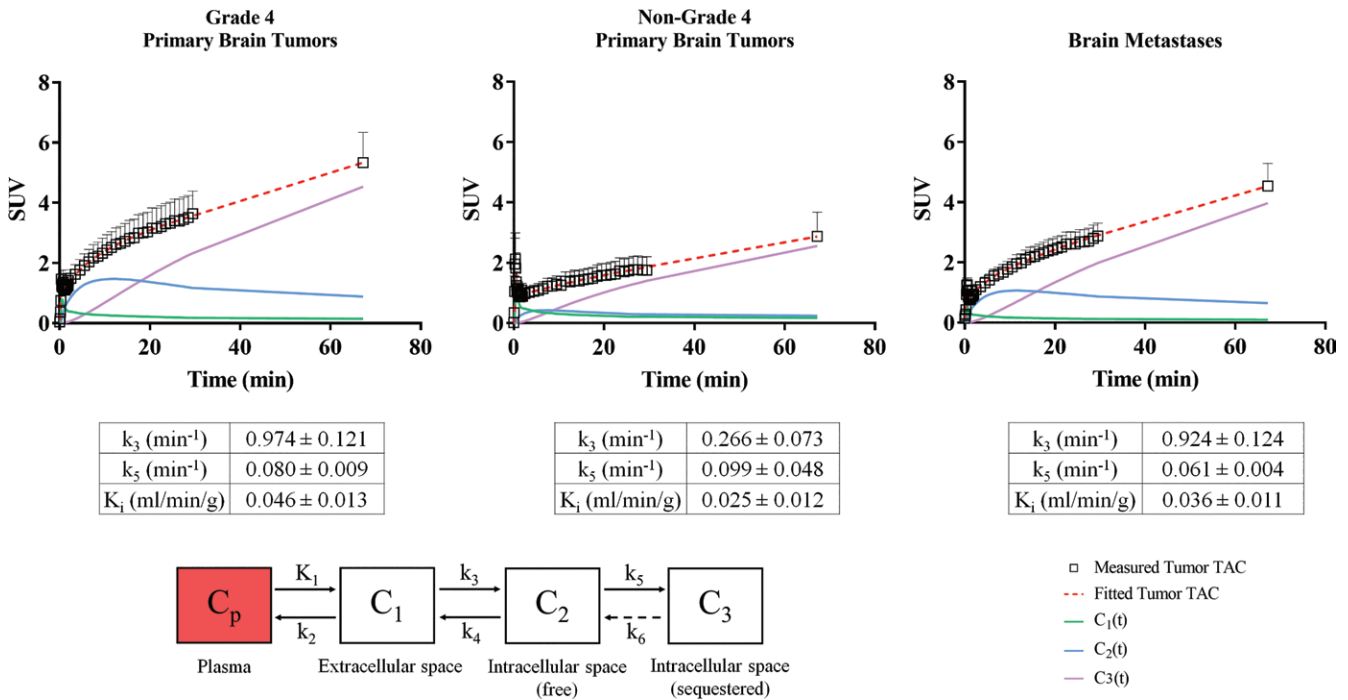


Figure 3: Compartmental model-fitted curves for the grade 4 primary brain tumor lesions (11 participants, 16 lesions), the non-grade 4 primary brain tumor lesions (six participants, 11 lesions), and the brain metastases (nine participants, 21 lesions). Error bars denote the standard error of the mean. C₁, C₂, and C₃ are the tracer concentrations in each tissue compartment. C_p is the tracer concentration in the plasma or blood compartment. K₁ = rate coefficient for transfer of tracer into the extracellular space from arterial plasma or blood compartment, k₂ = rate constant for transfer of tracer out of the extracellular space and into arterial plasma or blood compartment, k₃ = rate constant for transfer of tracer into the cell via system x_c⁻ from the extracellular space, k₄ = rate constant for transfer of tracer out of the cell and into the extracellular space, k₅ = sequestration rate constant of tracer into amino acid pools within the cell, K₁ = net influx rate constant of tracer uptake into tissue, SUV = standardized uptake value, TAC = time-activity curve.

Table 3: Estimated ¹⁸F-FSPG Kinetic Parameters

Kinetic Parameter*	Primary Brain Tumors		Brain Metastases
	Grade 4	Non-Grade 4	
K ₁ (mL/min/g)	0.475 ± 0.064	1.466 ± 0.157	0.575 ± 0.087
k ₂ (min ⁻¹)	3.798 ± 0.858	9.222 ± 0.812	6.637 ± 1.513
k ₃ (min ⁻¹)	0.974 ± 0.121	0.266 ± 0.073	0.924 ± 0.124
k ₄ (min ⁻¹)	0.110 ± 0.015	0.065 ± 0.054	0.067 ± 0.008
k ₅ (min ⁻¹)	0.080 ± 0.009	0.099 ± 0.048	0.061 ± 0.004
K ₁ (mL/min/g)	0.046 ± 0.013	0.025 ± 0.012	0.036 ± 0.011

Note.—Data are estimated parameter values ± standard errors. The number of participants and lesions in each group are as follows: grade 4 = 11 participants with 16 lesions, non-grade 4 = six participants with 11 lesions, and brain metastases = nine participants with 21 lesions.

* The rate constants describe the fraction of substance in one compartment being transported to another compartment per unit time. K₁ = rate coefficient for transfer of tracer into the extracellular space from arterial plasma or blood compartment, k₂ = rate constant for transfer of tracer out of the extracellular space and into arterial plasma or blood compartment, k₃ = rate constant for transfer of tracer into the cell via system x_c⁻ from the extracellular space, k₄ = rate constant for transfer of tracer out of the cell and into the extracellular space, k₅ = sequestration rate constant of tracer into amino acid pools within the cell, and K₁ = net influx rate constant of tracer uptake into tissue.

outcome groups, the kinetic parameter ΔK₁ performed slightly better (Fig 5). Table E8 (online) lists a summary of the estimated kinetic parameters between the good and poor lesion outcome subgroups within the cohort of participants with grade 4 primary brain tumors.

Kinetic Curve Assessment

The mean ¹⁸F-FSPG lesion TACs for participants with grade 4 brain tumor with good and poor lesion outcomes were significantly different from one another (F test, P < .001) (see Fig E7 [online]). A two-phase association model was used to fit the curves, whereby the lesion TAC was estimated as a sum of a fast and slow exponential decay. The TACs of participants with grade 4 tumors and a good lesion outcome at follow-up reached the plateau faster, and the absolute SUVs were lower than those in participants with a poor lesion outcome. In the participants with lesions with poor outcomes, there was a persistent rise in the ¹⁸F-FSPG lesion TAC, with a plateau that would occur later in time and at a higher SUV. Simulated projections of the curves over time to reach their plateaus are shown in Figure E8 (online). In addition, the mean ¹⁸F-FSPG TBR curves for the participants with grade 4 tumor as stratified by lesion outcome are presented in Figure E9 (online).

In Figure E10 (online), the plots show the mean ¹⁸F-FSPG TACs of the lesions in all participants with primary brain

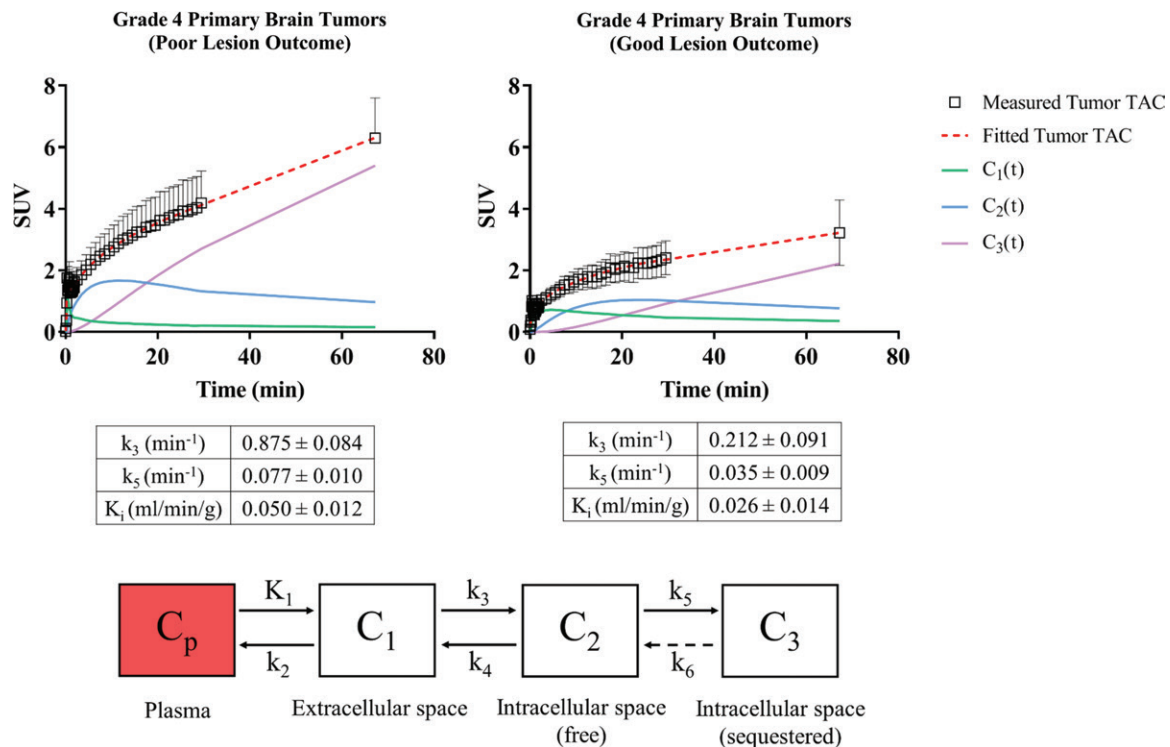


Figure 4: Compartmental model-fitted curves for grade 4 primary brain tumor lesions as stratified by lesion outcome (determined with follow-up MRI and/or pathologic examination). There were 11 grade 4 lesions in the poor lesion outcome group and five grade 4 lesions in the good lesion outcome group. Error bars denote the standard error of the mean. K_1 = rate coefficient for transfer of tracer into the extracellular space from arterial plasma or blood compartment, k_2 = rate constant for transfer of tracer out of the extracellular space and into arterial plasma or blood compartment, k_3 = rate constant for transfer of tracer into the cell via system x_c^- from the extracellular space, k_4 = rate constant for transfer of tracer out of the cell and into the extracellular space, k_5 = sequestration rate constant of tracer into amino acid pools within the cell, K_i = net influx rate constant of tracer uptake into tissue, SUV = standardized uptake value, TAC = tumor-activity curve.

tumors ($n = 17$) as stratified by their clinical outcome at follow-up. When comparing the two model curves using the F test, significant differences were observed ($P < .05$).

For the brain metastases group, there were no significant differences ($P > .05$) between the poor and good lesion outcome curves (Figs E11 and E12 [online]), as there was considerable overlap between the curves, especially during the 0–30-minute period.

ROC Curve Analysis

ROC curve analysis to evaluate the ability of ^{18}F -FSPG SUV_{max} and TBR (at WB timepoint) to differentiate good and poor lesion outcomes in the primary brain tumor group showed an area under the ROC curve (AUC) of 0.62 ($P = .32$) for SUV_{max} and 0.60 ($P = .42$) for TBR. When evaluating grade 4 primary brain tumors only, the AUC was 0.69 ($P = .23$) for SUV_{max} and 0.70 ($P = .21$) for TBR, respectively (Fig E13 [online]).

Figure 6 shows the ROC results comparing ΔK_i and $\Delta \text{SUV}_{\text{max}}$ in the grade 4 primary brain tumors and the entire primary brain tumor group. For grade 4 brain lesions, the AUC was 0.91 ($P = .01$) for both the ΔK_i and $\Delta \text{SUV}_{\text{max}}$ metrics. For ΔK_i or $\Delta \text{SUV}_{\text{max}}$, the sensitivity was 91% (10 of 11; 95% CI: 59, 100) in predicting the poor lesion outcome subgroup and the specificity was 80% (four of five; 95% CI: 28, 99) in predicting

the good lesion outcome subgroup. The overall accuracy for both decision metrics was 88% (14 of 16; 95% CI: 62, 98).

When all primary brain cancer lesions were pooled, the AUC was 0.91 ($P = .001$) for ΔK_i and 0.83 ($P = .01$) for $\Delta \text{SUV}_{\text{max}}$. For ΔK_i , the sensitivity was 95% (19 of 20; 95% CI: 75, 100), specificity was 71% (five of seven; 95% CI: 29, 96), and overall accuracy was 89% (24 of 27; 95% CI: 71, 98). For $\Delta \text{SUV}_{\text{max}}$, the sensitivity was 85% (17 of 20; 95% CI: 62, 97), specificity was 71% (five of seven; 95% CI: 29, 96), and overall accuracy was 81% (22 of 27; 95% CI: 62, 94).

Discussion

This study investigated the potential clinical role of (4S)-4-(3-[^{18}F]fluoropropyl)-L-glutamate (^{18}F -FSPG) PET/CT in the evaluation of primary brain tumors and brain metastases. The rationale behind the development of this radiopharmaceutical lies in the crucial role played by the cystine-glutamate exchanger in the protection against reactive oxygen species, which confers a survival advantage to tumor cells. ^{18}F -FSPG differs from other tracers because its uptake is associated with adaptations of the tumor cells to oxidative stress, thus exploring a different aspect of tumor biology.

Our study showed that ^{18}F -FSPG has high TBR in primary brain tumors and brain metastases (range: 2.6–150.3)

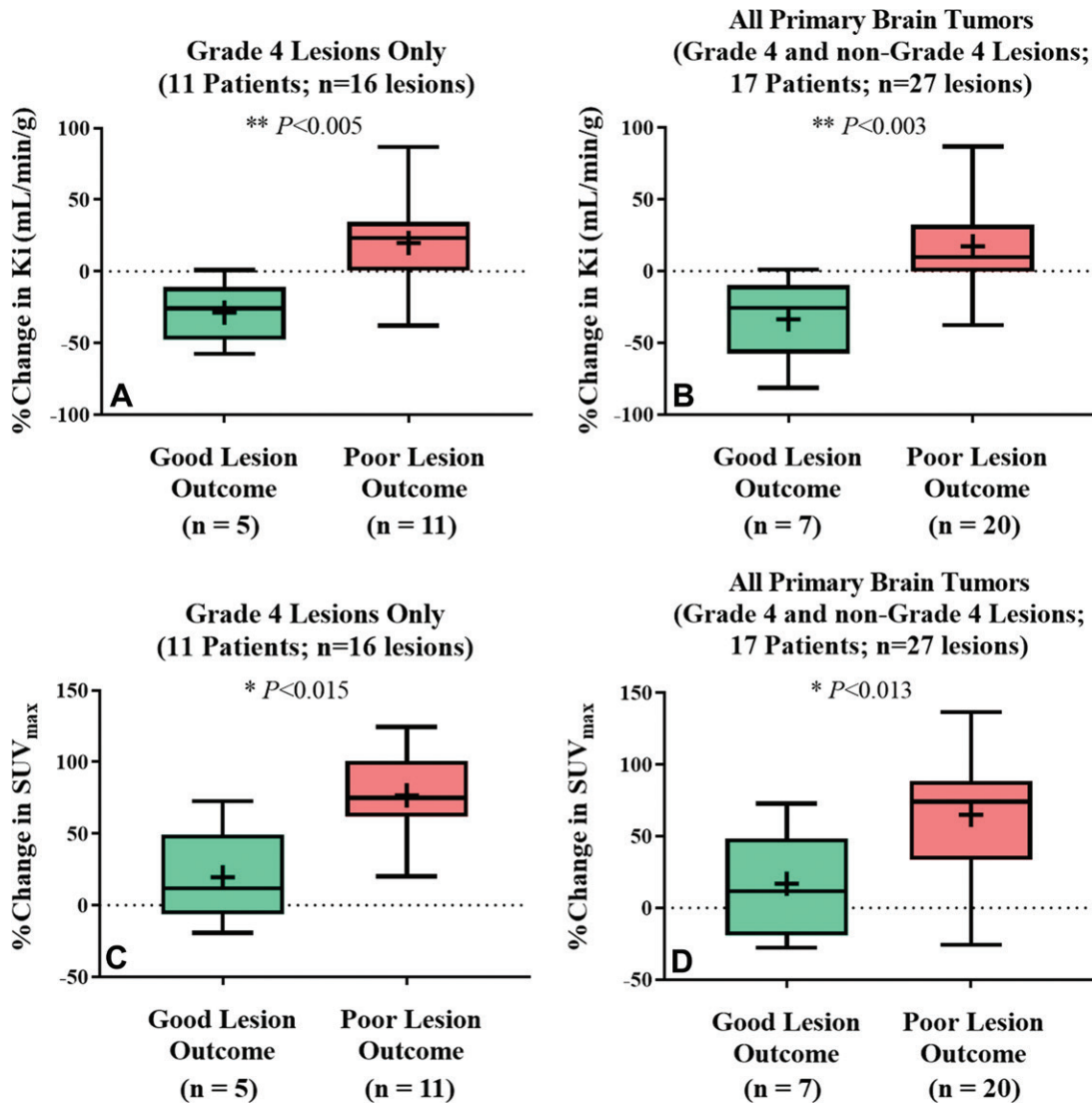


Figure 5: Box-and-whisker plots show the percentage change in (4S)-4-(3-[¹⁸F]fluoropropyl)-L-glutamate (¹⁸F-FSPG) influx rate constant (K_i) and maximum standardized uptake (SUV_{max}) for grade 4–only lesions (**A** and **C**) and grade 4 and non–grade 4 lesions pooled together (**B** and **D**). A plus sign (+) denotes the mean value in the box plots. The Student *t* test was used for group mean comparisons.

and negligible uptake in healthy brain parenchyma, thus allowing a clear delineation of the tumor—an important advantage of this PET tracer. The majority of grade 4 lesions (seven of nine) showed moderate or strong-diffuse staining for the xCT subunit of the x_c⁻ system, whereas all the non–grade 4 lesions either showed diffuse-weak staining or no staining at all. The fact that two of nine grade 4 tumors showed weak-diffuse or intense-focal staining on IHC could be due to the intrinsic limitations of tissue sampling. The use of a specific in vivo imaging marker, such as ¹⁸F-FSPG, could overcome this limitation by capturing the heterogeneity of the tumor lesion noninvasively. Within the grade 4 group, two participants with low ¹⁸F-FSPG uptake were treated with an anti-angiogenic drug before their scan (participants 8 and 12). The effects of systemic antiangiogenic treatments on radiopharmaceutical uptake, as well as those of radio-chemotherapy treatments, are not known at this time and need further investigation.

In our study, we included participants with metastatic disease with four different primary tumor types. The four metastatic brain lesions for which pathologic samples were available showed moderate or strong diffuse staining, and their ¹⁸F-FSPG uptake was highly variable. A possible explanation for this may be that these participants were treated with a wide combination of treatments including surgery, whole-brain radiation therapy, stereotactic radiosurgery, BRAF inhibitors, and radio-chemotherapy up to 4 weeks before the ¹⁸F-FSPG PET scan. The effects of all these therapies on ¹⁸F-FSPG uptake are unknown but may well have resulted in the heterogeneous radiopharmaceutical distribution that was observed. Our IHC findings, together with our initial quantitative assessment, suggest the importance of focusing future studies first on grade 4 primary brain tumors, then perhaps on more specific solid tumors that result in brain metastasis.

We also showed that different lesions varied in their temporal patterns of uptake on the dynamic PET scans. In

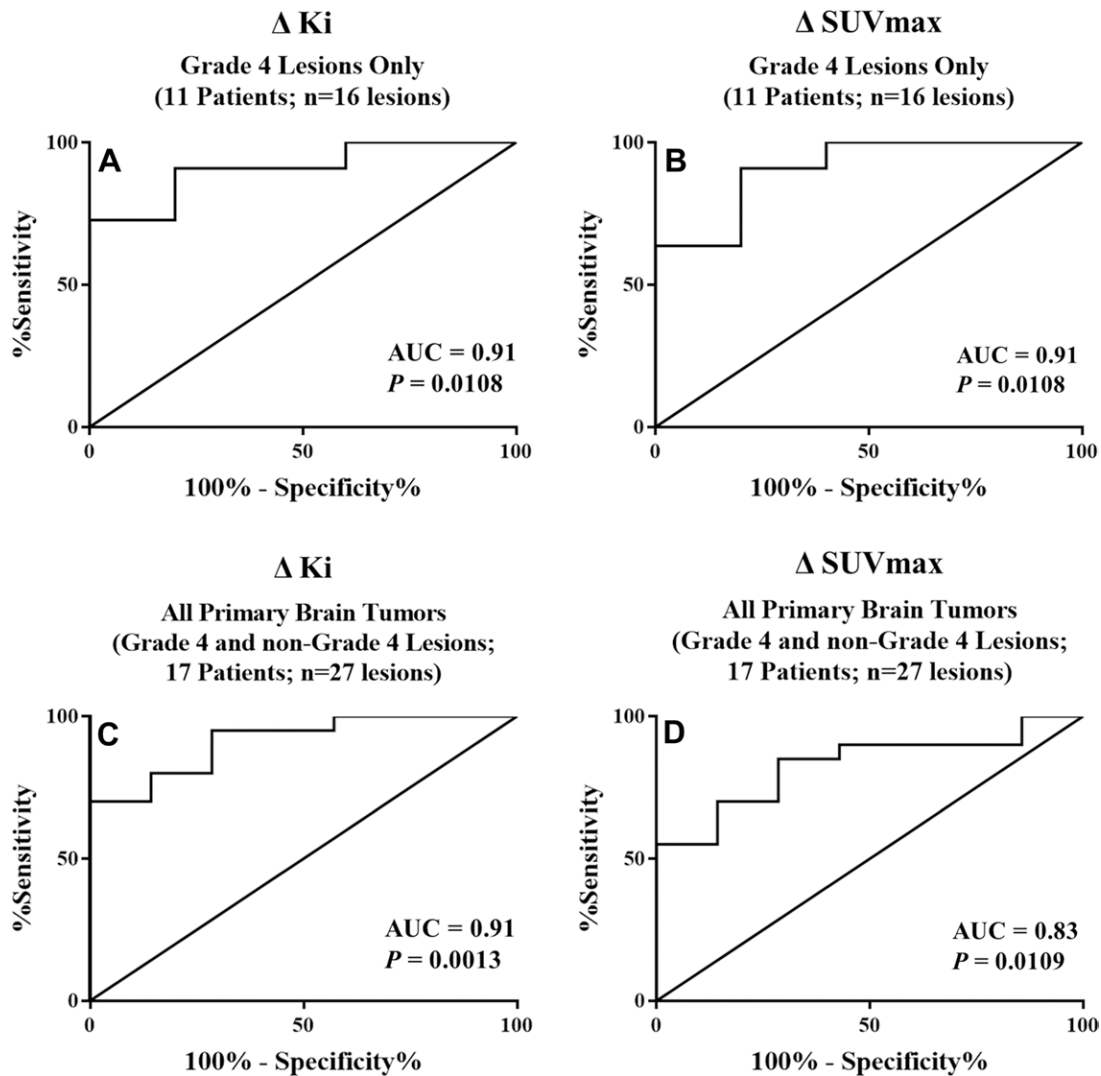


Figure 6: Receiver operating characteristic (ROC) curve analysis is comparing the decision measures **(A, C)** ΔK_i and **(B, D)** ΔSUV_{max} in the grade 4–only primary brain tumors and the entire primary brain tumor group (grade 4 and non–grade 4 brain lesions pooled together). AUC = area under the ROC curve, ΔK_i = percentage change between the K_i value estimated using the 30-minute dynamic PET data and the K_i value estimated using the dynamic plus whole-body PET data. ΔSUV_{max} = percentage change in maximum standardized uptake value of the brain lesion between the dynamic PET scan (last frame) and whole-body PET scan.

general, more aggressive tumor lesions tended to accumulate ^{18}F -FSPG during the dynamic scan faster than less aggressive ones. Relative changes in K_i and SUV were most predictive of lesion outcome. Multi-time-point analysis showed that the relative changes in K_i and SUV_{max} were different between the lesions with good and poor outcomes. For grade 4 primary brain lesions, the overall predictive accuracy was 87.5% for both ΔK_i and ΔSUV_{max} . Across all primary brain tumors, the overall predictive accuracy was 89% and 81% for ΔK_i and ΔSUV_{max} , respectively. This finding is noteworthy because ^{18}F -FSPG PET/CT enabled early prediction of lesion outcome that was confirmed by follow-up MRI performed, in many cases several months after the ^{18}F -FSPG PET scan. In the brain metastases group, there were no significant differences between the poor and good lesion outcome curves, possibly due to the inherent different biology of brain metastases.

For participants with grade 4 primary brain tumors with a good lesion outcome, their lesion curves plateaued faster and had a lower absolute uptake value than those with a poor outcome. In the latter group, however, there was a persistent rise in the ^{18}F -FSPG lesion TAC, with a plateau that occurred later. In future studies, instead of imaging out to later times to reach the ^{18}F -FSPG tumor plateau, a bolus plus a constant infusion could be used to reach the plateau earlier (26).

The kinetic curves of ^{18}F -FSPG differ from those reported for other amino acid–based PET tracers. The kinetic analysis of ^{18}F L-3,4-dihydroxyphenylalanine (^{18}F -FDOPA) uptake in brain tumors was first reported by Schiepers et al (27). They showed that after an early maximum, the ^{18}F -FDOPA uptake curves of high-grade tumors decreased steeply, whereas low-grade tumors had a slow decline. The authors of that study did not report on any correlations to patient outcome. Albert et al (28) showed that ^{18}F -fluoroethyltyrosine

(¹⁸F-FET) tumor uptake kinetics exhibited increasing TACs in low-grade gliomas, while high-grade gliomas typically showed highest tracer uptake within the first 5–15 minutes with subsequent decrease. A preliminary evaluation by Galldiks et al (29) indicated that radiation necrosis typically showed a steadily increasing ¹⁸F-FET curve pattern, whereas curve patterns in recurrent metastases typically showed an early peak followed by either a plateau or a constant descent—a different behavior compared with ¹⁸F-FSPG.

Moreover, the role of the blood-brain barrier must be considered. Several methods and biologic markers to assess extravasation across or disruption of the blood-brain barrier have been proposed (30,31). The ability of ¹⁸F-FSPG to cross the intact blood-brain barrier or the degree of disruption needed for uptake requires further investigation. However, there was at least one lesion (participant 2) that was nonenhancing on MRI and exhibited mild ¹⁸F-FSPG uptake (ie, slightly higher than that in healthy tissue). This needs to be explored further.

Limitations of our study include the relatively small cohort of participants involved and the heterogeneity of tumor type, particularly for the subgroup analysis. Our analyses also did not take into account the clustering of multiple lesions within patients. Another limitation was the number of available tissue samples for the IHC and pathologic assessments (19 of 48 lesions). Additionally, not all lesions were excised within a month from the ¹⁸F-FSPG PET scan and analyzed for x_c⁻ staining. In some cases, the time difference between tissue sample collection used for the histopathologic and IHC analyses and the ¹⁸F-FSPG PET scan was more than 1 year (Table E2 [online]). This hampers the ability to draw clear conclusions from the IHC analysis due to the evolving nature of the malignant process.

The use of different standard-of-care treatments between ¹⁸F-FSPG PET/CT and the follow-up evaluation in most participants, while a clinical reality, is not ideal because the prediction of lesion outcome can be influenced by the therapeutic intervention. This requires additional investigation. Future validation of our results in larger and more homogeneous groups of participants are needed, and further studies are warranted to confirm the ability of ¹⁸F-FSPG PET/CT to help predict lesion outcome as well as to define its potential role in the clinical management of patients with brain tumors. Given the exploratory nature of this research, these limitations were somewhat unavoidable, but the goal was to find a signal worth pursuing for subsequent research, which was achieved.

In conclusion, our study showed that (4S)-4-(3-[¹⁸F] fluoropropyl)-L-glutamate (¹⁸F-FSPG) is taken up by both primary brain tumors and brain metastases, with a high tumor-to-background ratio. Moreover, relative changes of ¹⁸F-FSPG PET parameters appear to be helpful in predicting lesion outcomes. These findings suggest a potentially important clinical role of imaging system x_c⁻ transporter activity with ¹⁸F-FSPG PET/CT in neuro-oncology.

Acknowledgments: We thank all the patients and their families who participated in this study and dedicate this work to them. In addition, we thank our referring physicians, clinical research coordinators, PET/CT technologists, and the radiochemistry staff. We are grateful to Frezghi Habte, PhD, for his technical assistance and Tie Liang, EdD, for her statistical support. This work is also dedicated to the

memory of Dr Sanjiv “Sam” Gambhir, our beloved leader, mentor, and friend, whose guidance was instrumental to the completion of this project. Sam’s extraordinary impact and enduring vision will live on in our hearts and minds and continue to guide our future work for years to come.

Author contributions: Guarantors of integrity of entire study, **M.W., I.S., E.S.M.**; study concepts/study design or data acquisition or data analysis/interpretation, all authors; manuscript drafting or manuscript revision for important intellectual content, all authors; approval of final version of submitted manuscript, all authors; agrees to ensure any questions related to the work are appropriately resolved, all authors; literature research, **M.W., I.S., G.Z., E.S.M.**; clinical studies, **M.W., I.S., R.M., N.H., G.Z., N.F., S.N., G.L., N.K., H.C.M., F.T.C., S.S.G., E.S.M.**; experimental studies, **M.W., M.J., G.Z., M.B., A.W.S., T.A., H.C.M., F.T.C., E.S.M.**; statistical analysis, **M.W., N.K., S.B., H.C.M., J.R.**; and manuscript editing, **M.W., I.S., A.P.F., N.F., S.N., G.L., N.K., A.W.S., L.M.D., H.C.M., F.T.C., S.S.G., E.S.M.**

Disclosures of conflicts of interest: **M.W.** No relevant relationships. **I.S.** No relevant relationships. **A.P.F.** No relevant relationships. **R.M.** No relevant relationships. **M.J.** Payment from Quality Care Solution. **N.H.** No relevant relationships. **G.Z.** Editorial board member, board membership on Subtle Medical; grants from NIH R01-EB025220, GE Healthcare sponsored research; payments from Biogen for advisory board for ARIA; payment to institution for various MR, PET, and AI patents; royalties from Cambridge University Press; stock options in Subtle Medical; travel/accommodations/meeting expenses from Subtle Medical. **N.F.** No relevant relationships. **S.N.** No relevant relationships. **G.L.** No relevant relationships. **N.K.** Payment from Life Molecular, Tegeler Str. 6-7; FSPG patents from Life Molecular Imaging. **M.B.** Patents from Life Molecular Imaging. **S.B.** No relevant relationships. **A.W.S.** FSPG patents from Life Molecular Imaging. **L.M.D.** FSPG patents from Life Molecular Imaging. **T.A.** No relevant relationships. **H.C.M.** No relevant relationships. **J.R.** No relevant relationships. **F.T.C.** Grant from Life Molecular Imaging; paid consultant for GE Healthcare; paid to help set up and promote clinical cyclotron and radiochemistry operation in Latin America for IQ Pharma; grant from the National Cancer Institute. **S.S.G.** Board membership from Life Molecular Imaging; consultancy for Life Molecular Imaging; grants from Life Molecular Imaging. **E.S.M.** Consultancy for AAA/Novartis; payment for lectures from AAA/Novartis; payment for development of educational presentations from Curium Pharma.

References

1. Cha S. Neuroimaging in neuro-oncology. *Neurotherapeutics* 2009; 6(3):465–477.
2. Ferguson SD. Malignant gliomas: diagnosis and treatment. *Dis Mon* 2011; 57(10):558–569.
3. Mabray MC, Barajas RF Jr, Cha S. Modern brain tumor imaging. *Brain Tumor Res Treat* 2015;3(1):8–23.
4. Shah AH, Snelling B, Bregy A, et al. Discriminating radiation necrosis from tumor progression in gliomas: a systematic review what is the best imaging modality? *J Neurooncol* 2013;112(2):141–152.
5. Jung JH, Ahn BC. Current Radiopharmaceuticals for Positron Emission Tomography of Brain Tumors. *Brain Tumor Res Treat* 2018;6(2):47–53.
6. Treglia G, Muoio B, Trevisi G, et al. Diagnostic Performance and Prognostic Value of PET/CT with Different Tracers for Brain Tumors: A Systematic Review of Published Meta-Analyses. *Int J Mol Sci* 2019;20(19):4669.
7. Koglin N, Mueller A, Berndt M, et al. Specific PET imaging of x_c⁻ transporter activity using a ¹⁸F-labeled glutamate derivative reveals a dominant pathway in tumor metabolism. *Clin Cancer Res* 2011;17(18):6000–6011.
8. Robert SM, Sontheimer H. Glutamate transporters in the biology of malignant gliomas. *Cell Mol Life Sci* 2014;71(10):1839–1854.
9. Pavlova NN, Thompson CB. The Emerging Hallmarks of Cancer Metabolism. *Cell Metab* 2016;23(1):27–47.
10. McCormick PN, Greenwood HE, Glaser M, et al. Assessment of Tumor Redox Status through (S)-4-(3-[¹⁸F]fluoropropyl)-L-Glutamic Acid PET Imaging of System x_c⁻ Activity. *Cancer Res* 2019;79(4):853–863.
11. Mosci C, Kumar M, Smolarz K, et al. Characterization of Physiologic ¹⁸F FSPG Uptake in Healthy Volunteers. *Radiology* 2016;279(3):898–905.
12. Smolarz K, Krause BJ, Graner FP, et al. (S)-4-(3-[¹⁸F]-fluoropropyl)-L-glutamic acid: an ¹⁸F-labeled tumor-specific probe for PET/CT imaging—dosimetry. *J Nucl Med* 2013;54(6):861–866.
13. Baek S, Choi CM, Ahn SH, et al. Exploratory clinical trial of (4S)-4-(3-[¹⁸F] fluoropropyl)-L-glutamate for imaging x_c⁻ transporter using positron emission tomography in patients with non-small cell lung or breast cancer. *Clin Cancer Res* 2012;18(19):5427–5437.
14. Baek S, Mueller A, Lim YS, et al. (4S)-4-(3-[¹⁸F]-fluoropropyl)-L-glutamate for imaging of x_c transporter activity in hepatocellular carcinoma using PET: preclinical and exploratory clinical studies. *J Nucl Med* 2013;54(1):117–123.

15. Chae SY, Choi CM, Shim TS, et al. Exploratory Clinical Investigation of (4S)-4-(3-¹⁸F-Fluoropropyl)-L-Glutamate PET of Inflammatory and Infectious Lesions. *J Nucl Med* 2016;57(1):67–69.
16. Cheng MF, Huang YY, Ho BY, et al. Prospective comparison of (4S)-4-(3-¹⁸F-fluoropropyl)-L-glutamate versus ¹⁸F-fluorodeoxyglucose PET/CT for detecting metastases from pancreatic ductal adenocarcinoma: a proof-of-concept study. *Eur J Nucl Med Mol Imaging* 2019;46(4):810–820.
17. Greenwood HE, McCormick PN, Gendron T, et al. Measurement of Tumor Antioxidant Capacity and Prediction of Chemotherapy Resistance in Preclinical Models of Ovarian Cancer by Positron Emission Tomography. *Clin Cancer Res* 2019;25(8):2471–2482.
18. Hoehne A, James ML, Alam IS, et al. [¹⁸F]FSPG-PET reveals increased cystine/glutamate antiporter (x_c⁻) activity in a mouse model of multiple sclerosis. *J Neuroinflammation* 2018;15(1):55.
19. Kavanaugh G, Williams J, Morris AS, et al. Utility of [¹⁸F]FSPG PET to Image Hepatocellular Carcinoma: First Clinical Evaluation in a US Population. *Mol Imaging Biol* 2016;18(6):924–934.
20. Magarik MA, Walker RC, Gilbert J, Manning HC, Massion PP. Intracardiac Metastases Detected by ¹⁸F-FSPG PET/CT. *Clin Nucl Med* 2018;43(1):28–30.
21. Martín A, Vázquez-Villoldo N, Gómez-Vallejo V, et al. In vivo imaging of system x_c⁻ as a novel approach to monitor multiple sclerosis. *Eur J Nucl Med Mol Imaging* 2016;43(6):1124–1138.
22. Mittra ES, Koglin N, Mosci C, et al. Pilot Preclinical and Clinical Evaluation of (4S)-4-(3-¹⁸F)Fluoropropyl)-L-Glutamate (¹⁸F-FSPG) for PET/CT Imaging of Intracranial Malignancies. *PLoS One* 2016;11(2):e0148628.
23. Ellingson BM, Bendszus M, Boxerman J, et al. Consensus recommendations for a standardized Brain Tumor Imaging Protocol in clinical trials. *Neuro Oncol* 2015;17(9):1188–1198.
24. Schiepers C, Chen W, Dahlbom M, Cloughesy T, Hoh CK, Huang SC. ¹⁸F-fluorothymidine kinetics of malignant brain tumors. *Eur J Nucl Med Mol Imaging* 2007;34(7):1003–1011.
25. Bertoldo A, Peltoniemi P, Oikonen V, Knuuti J, Nuutila P, Cobelli C. Kinetic modeling of [¹⁸F]FDG in skeletal muscle by PET: a four-compartment five-rate-constant model. *Am J Physiol Endocrinol Metab* 2001;281(3):E524–E536.
26. Carson RE, Channing MA, Blasberg RG, et al. Comparison of bolus and infusion methods for receptor quantitation: application to [¹⁸F]cyclofoxy and positron emission tomography. *J Cereb Blood Flow Metab* 1993;13(1):24–42.
27. Schiepers C, Chen W, Cloughesy T, Dahlbom M, Huang SC. ¹⁸F-FDOPA kinetics in brain tumors. *J Nucl Med* 2007;48(10):1651–1661.
28. Albert NL, Winkelmann I, Suchorska B, et al. Early static ¹⁸F-FET-PET scans have a higher accuracy for glioma grading than the standard 20-40 min scans. *Eur J Nucl Med Mol Imaging* 2016;43(6):1105–1114.
29. Galldiks N, Langen KJ, Pope WB. From the clinician's point of view - What is the status quo of positron emission tomography in patients with brain tumors? *Neuro Oncol* 2015;17(11):1434–1444.
30. Kong Z, Yan C, Zhu R, et al. Imaging biomarkers guided anti-angiogenic therapy for malignant gliomas. *Neuroimage Clin* 2018;20:51–60.
31. Hutterer M, Hattingen E, Palm C, Proescholdt MA, Hau P. Current standards and new concepts in MRI and PET response assessment of antiangiogenic therapies in high-grade glioma patients. *Neuro Oncol* 2015;17(6):784–800.